ACS APPLIED MATERIALS & INTERFACES

Research Article

www.acsami.org

Confinement of Ferroelectric Domain-Wall Motion at Artificially Formed Conducting-Nanofilaments in Epitaxial $BiFeO_3$ Thin Films

Woo-Hee Kim,*[,†] Jong Yeog Son,*[,‡] and Hyun Myung Jang[§]

[†]Department of Chemical Engineering, Stanford University, 381 North-South Mall, Stanford, California 94305, United States

[‡]Department of Applied Physics, College of Applied Science, Kyung Hee University, 1732 Deogyeong-daero, Giheung-Gu, Yongin-City 446-701, Korea

[§]Department of Materials Science and Engineering, and Department of Physics, Pohang University of Science and Technology (POSTECH), 77 Cheongam-Ro, Nam-Gu, Pohang 790-784, Korea

Supporting Information

ABSTRACT: We report confinement of ferroelectric domain-wall motion at conducting-nanofilament wall in epitaxial $BiFeO_3$ thin film on Nb-doped $SrTiO_3$ substrate. The $BiFeO_3$ film exhibited well-defined ferroelectric response and unipolar resistive switching behavior. We artificially formed conducting-nanofilaments in the $BiFeO_3$ via conducting atomic force microscope techniques. The conducting-nanofilament wall, which does not possess any ferroelectric polarization, is then able to block domain propagation. Consequently, we demonstrate that the domain-wall motion is effectively confined within the conducting-nanofilament wall during polarization switching. This significant new insight potentially gives an opportunity for the artificial manipulation of nanoscale ferroelectric domain.

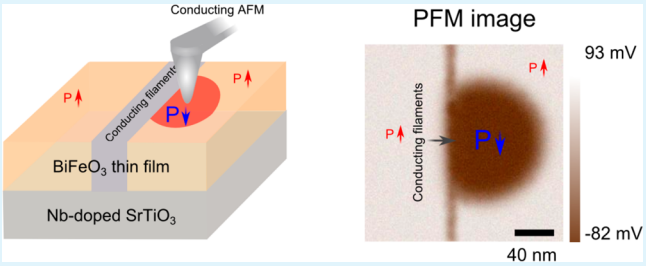

KEYWORDS: *$BiFeO_3$ thin film, ferroelectric response, resistive switching, conducting-filament, domain-wall motion*

INTRODUCTION

Until recently, multiferroic materials, which simultaneously exhibit both ferroelectricity and ferromagnetism with coupled electric and magnetic order parameters, have been a subject of intensive scientific investigation due to their interesting physical properties and potential device applicability including the emerging field of spintronics, data-storage media, and multiple-state memories.[1−3] Through the exploration of these properties in many materials, $BiFeO_3$ (BFO) has stood out as the most promising candidate, since it was still known to be the only ABO_3-type simple perovskite with ferroelectricity and antiferromagnetism coexisting at room temperature.[4−7] Nevertheless, a large leakage current, which originates from the presence of oxygen vacancies created in the film growth process, hinders its potential applications as the ferroelectric material. Accordingly, numerous attempts have been devoted to reducing the leakage current; these have primarily focused on site-engineering using substitution of some elements at the A-site.[8−10]

Contrastively, as far as other applications in the BFO films are concerned, the oxygen vacancies can be used to some extent in conjunction with ferroelectric polarization. In recent years, the BFO has exhibited a great potential in nonvolatile resistance random access memory (RRAM) device.[11−13] Particularly, Liu et al. reported that both unipolar and bipolar resistive switching phenomena, which are associated with conducting nanofilaments consisting of oxygen vacancies, were simultaneously observed in the BFO-based RRAM capacitors.[14] More interestingly, formation of a RRAM conducting nanofilament wall in the BFO film seems possible by using a conducting atomic force microscope (CAFM) technique. Since then, subsequent surface measurements using the CAFM enables us to observe the conducting nanofilaments pertaining to the RRAM switching phenomena. In recent literature, on the basis of the CAFM methodology, we have demonstrated the formation of conducting nanobits and subsequent characterizations of resistive switching for NiO and HfO_2 thin films.[15−17]

In this report, therefore, we comprehensively investigated ferroelectric domains and RRAM conducting nanofilaments in an epitaxially grown BFO thin film grown on an Nb-doped $SrTiO_3$ (Nb:STO) substrate. The BFO films exhibited the ferroelectric polarization with a well-defined saturation and the unipolar resistive switching behavior. In addition, the controllable formation of conducting nanofilament was demonstrated in the BFO films by using a biased CAFM tip. Based on the above key features, we observed an interesting phenomenon that the ferroelectric domain-wall motion during the polarization switching is confined within the conducting nanofilament wall.

Received: December 10, 2013
Accepted: April 21, 2014
Published: April 21, 2014

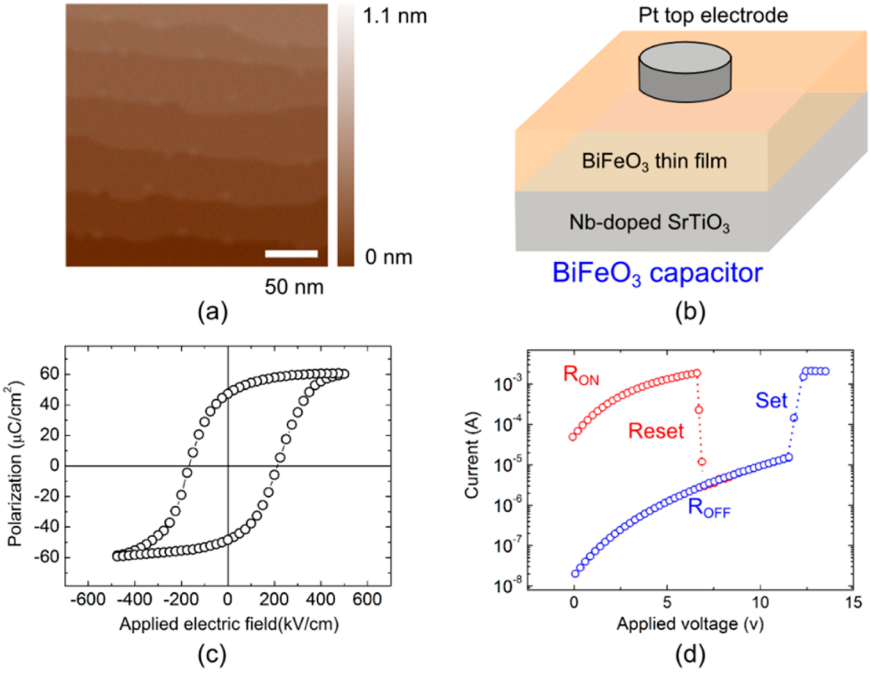

Figure 1. (a) AFM image of the BFO thin film on the Nb:STO substrate, (b) schematic illustration of the BFO capacitor (Pt/BFO/Nb:STO) structure, (c) ferroelectric hysteresis loop (P−E), and (d) bistable resistive switching characteristic of the Pt/BFO/Nb:STO capacitor.

EXPERIMENTAL SECTION

2.1. $BiFeO_3$ Thin Film Deposition and Capacitor Fabrication. For this study, a $BiFeO_3$ bulk target was prepared by using a conventional solid-state reaction method. High purity, commercially available powders of all the chemicals, that is, Bi_2O_3 (99.99% pure) and Fe_2O_3 (99.99%) (MTI Co., U.S.A.), were mixed in molar ratios. The mixtures were well ground, pelletized, and fired in an air environment at 400 °C for 10 h, at 700 °C for 12 h, and finally at 880 °C for 5 h with intermediate grinding. Then, BFO thin films were epitaxially grown by pulsed laser deposition (PLD) on a (001) oriented Nb-doped $SrTiO_3$ (Nb:STO) substrate with resistivity of ∼0.001 Ω·cm at the Nb-doping level of ∼1 wt %, which has an atomically flat surface with well-aligned terraces formed by HF treatment and annealing at 1000 °C for 1 h. A KrF excimer laser with a wavelength of 248 nm and an energy density of 0.5 J/cm^2 was focused onto the targets. The distance between the target and substrate was maintained to be ∼4 cm. Once the base pressure reached ∼5 × 10^{-7} Torr, the substrate temperature was set to 800 °C with an oxygen partial pressure of 100 mTorr. After deposition, all thin films were subject to slow cooling down to room temperature at a rate of 100°C/h in an oxygen ambient at 300 Torr. To prepare circular-shaped top electrodes with a radius of 100 μm, 100 nm-thick Pt layer was deposited on the BFO film by RF magnetron sputtering through a dot-patterned shadow mask, and then, subsequent annealing was carried out at 400 °C for 5 min in ambient air.

2.2. Characterizations. The thickness of the BFO film was 50 nm unless otherwise noted, which was measured by taking a cross-sectional image of the sample using a scanning electron microscope (SEM). For the structural determination of the thin films, the X-ray diffraction data of $\theta-2\theta$ scan and Φ-scan were obtained by powder (Rigaku, Cu Kα radiation) and four-circle (Huber goniometer, Cu Kα radiation) X-ray diffractometers. The surface morphology and root-mean-square (RMS) roughness of the BFO thin film was observed by atomic force microscope (AFM) measurement with a VEECO Dimension 3100 AFM system. Besides that, the RRAM conducting-filament and ferroelectric polarization switching in the BFO thin film were elaborately monitored by various AFM characterizations such as CAFM, piezoresponse force microscope (PFM) and Kelvin force microscope (KFM). The ferroelectric hysteresis loop of the BFO thin film capacitors was measured by an RT66A (Radiant Technologies, Inc.) test system, and the resistive switching characteristic was evaluated by Keithley 4200 semiconductor characterization system.

RESULTS AND DISCUSSION

Figure 1a shows an AFM image of the BFO thin film grown on the Nb:STO substrate. Atomically flat (RMS roughness <5 Å) and clear surface steps with an interval of about 50 nm were clearly observed due to its layer-by-layer growth. The $\theta-2\theta$ X-ray diffraction patterns indicate that the BFO films on the Nb:STO(001) is epitaxially grown without any secondary phase along the substrate orientation [Figure S1a in the Supporting Information (SI)]. The in-plane epitaxial relationship between the Nb:STO substrate and the BFO films was further investigated by 360° Φ-scan for (111) diffraction of Nb:STO(001) and BFO (Figure S1b in the SI). Perfectly overlapped four peaks with 90° separation of BFO and Nb:STO(111) peaks manifest the cube-on-cube epitaxial relationship of BFO[100]//STO[100] and BFO(001)//STO(001). We then prepared the Pt/BFO/Nb:STO-structured capacitor, which is schematically shown in Figure 1b, to examine the ferroelectric polarization and resistive switching behavior. First, the ferroelectric polarization versus electric field (P−E) characteristic was evaluated at a measurement frequency of 10 kHz in Figure 1c. The P−E hysteresis loop of the BFO thin film capacitor exhibited a high remnant polarization of ∼50 μC/cm^2 ($2P_r$ ∼ 100 μC/cm^2) with a coercive electric field (E_c) of ∼200 kV/cm. Next, to further confirm the resistive switching behavior with a carefully limited compliance current (I_{COMP}) of 2 mA, we investigated current−voltage ($I-V$) characteristics of the BFO thin film capacitor. The BFO RRAM capacitor exhibited a bistable resistive switching behavior with a typical unipolar resistive switching characteristic as presented in Figure 1d. Initially, we formed a conducting path in the BFO film with a forming bias of about 15.5 V. In the following voltage sweep measurements, the R_{ON} state goes back to the R_{OFF} state above the RESET bias of ∼6.6 V. This R_{OFF} state switches again to the

dx.doi.org/10.1021/am501630k | ACS Appl. Mater. Interfaces 2014, 6, 6346−6350

R_{ON} state above the SET bias of ~11.7 V. The transformed low resistance state in the BFO film is maintained even with decreasing the voltage down to zero. The bistable resistance states of the Pt/BFO/Nb:STO capacitor could be reproducible for more than 200 DC sweep cycles and remain almost unchanged over a period of 10^5 s (Figure S2 in the SI). In other words, it means that reliable endurance and retention properties of the BFO RRAM capacitor were demonstrated.

Figure 2a illustrates the BFO thin film with opposite ferroelectric polarization configuration on each side of a

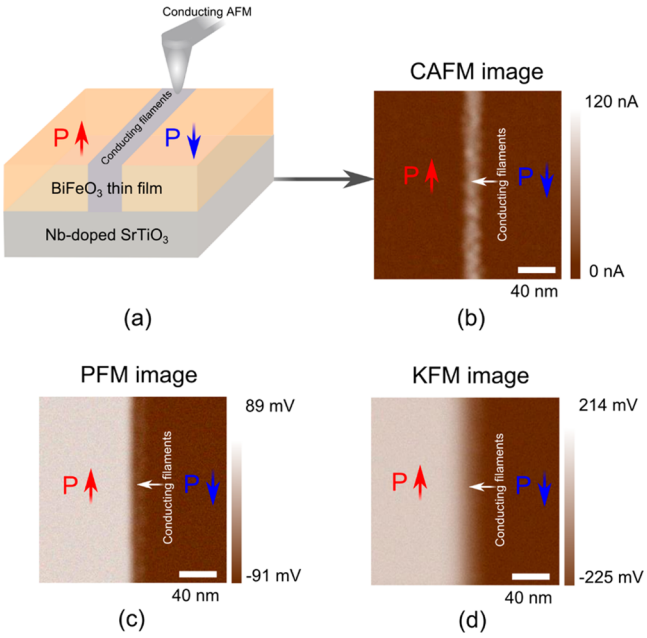

Figure 2. (a) Schematic illustration of the BFO thin film with opposite ferroelectric polarization configuration around the conducting nanofilament wall formed by a biased CAFM tip; (b) CAFM, (c) PFM, and (d) KFM images of the BFO thin film in the vicinity of the CAFM-formed conducting nanofilament wall.

conducting nanofilament line. First, we arranged upwardly polarized domains on the surface by applying a bias of −5 V between the PFM tip and the substrate. Then, a line pattern of conducting nanofilament was artificially formed across the upwardly polarized region by using the CAFM technique with the forming bias of 15.5 V. We applied a bias of +5 V between the PFM tip and the substrate again to reverse the domain direction on the right side of that conducting nanofilament line, and thereby, the formation of ferroelectric domain regions polarized upwardly and downwardly, respectively, around the conducting line pattern was achieved. The following CAFM image clearly shows the conducting nanofilament wall with the width of about 20 nm (a bright line in Figure 2b). Additionally, Figure 2c shows a PFM image of the BFO thin film in which upwardly and downwardly polarized domains are clearly separated by the conducting nanofilament formed by a biased CAFM tip. It is noted that the brightness of the conduction-filament is nearly intermediate between upwardly (left) and downwardly (right) polarized regions, implying the absence of the dominant polarization direction in the conducting nanofilament. A KFM image in the vicinity of the conducting nanofilament is presented in Figure 2d, showing upward and downward polarizations likewise. In contrast to the PFM image, however, it is difficult to clearly observe the conducting nanofilament wall due to relatively lower resolution of KFM than that of PFM.[18,19]

To further clarify the existence of the artificially formed conducting nanofilaments between the opposite polarization regions, we comparatively presented surface potential differences by complementary PFM and KFM measurements in the vicinity of the conductive line, as pictorially shown in Figure 3a.

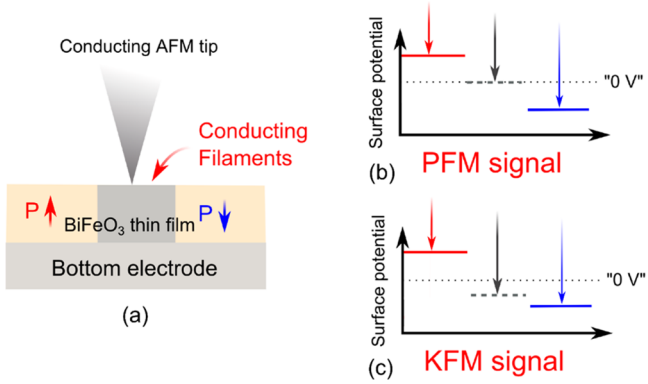

Figure 3. (a) Cross-sectional illustration of the BFO thin film with opposite ferroelectric polarization configuration around the conducting nanofilament wall formed by a biased CAFM tip; (b) PFM, and (c) KFM surface potential profiles in the vicinity of the CAFM-formed conducting nanofilament wall.

Here, the sign of the (+) surface potential on the left-hand-side domain is opposite to that (−) on the right-hand-side domain as well, because both sides of the conducting filament line have opposed polarizations with upward and downward direction, respectively. However, the value of the surface potential on the conducting filament line in the KFM measurement is a little bit different from that in the PFM measurement. More specifically, the PFM can reflect local piezoelectric response properties by applying the bias as the direct contact mode of the tip. Once the highly leaky surfaces such as the conducting filaments are scanned, all the charges induced by the voltage applied to the PFM tip are flowing into the conducting nanofilaments with high conductivity, and thereby, the surface potential is observed to be "0" (Figure 3b). On the contrary, to measure the surface potential by the non-contact KFM measurement, a reference AC bias is applied to the KFM tip, then, image charges are induced only at the conducting nanofilament region. Accordingly, the negative surface potential of the KFM signal is expected, reflecting attractive force between the surface potential of the image charges on the surface of the conducting filament and the charges induced at the KFM tip (Figure 3c).[15]

Figure 4a schematically depicts a conducting nanofilament wall built up between upwardly polarized domains by the same CAFM method above. For this, we arranged upwardly polarized domains on the surface by applying a bias of −5 V between the PFM tip and the substrate as well, and then, the conducting nanofilament line was scanned across the upwardly polarized region by the CAFM technique with the forming bias of 15.5 V. In the PFM measurement, likewise, the surface potential on the conducting nanofilament should be "0", whereas that on both the parallel domains in the vicinity of the conducting line should have (+) surface potential (Figure 4b). Figure 4c shows a PFM image of upwardly polarized parallel domains separated by the conducting nanofilament wall. Both sides of the polarized regions show a brighter color in the PFM image

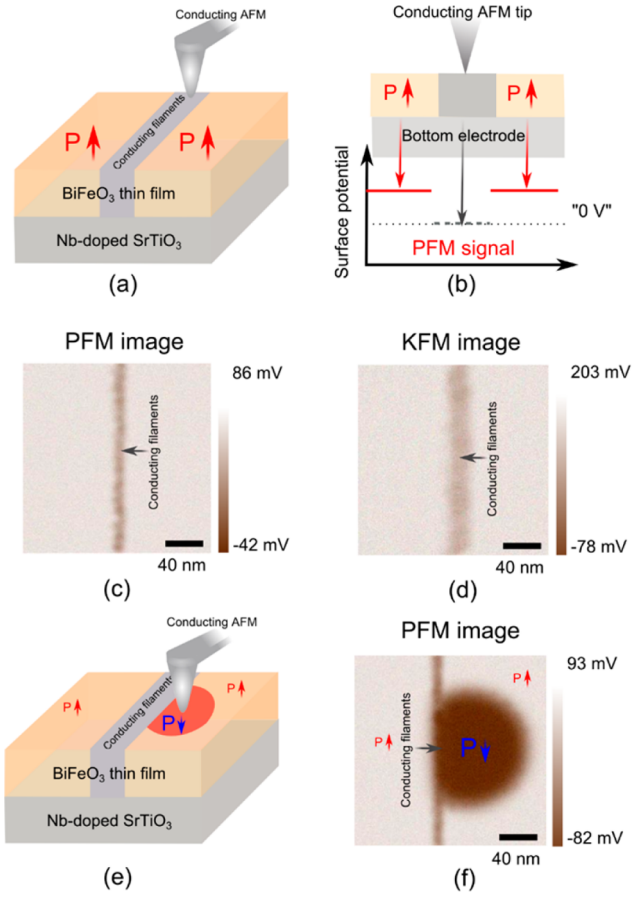

Figure 4. (a) Schematic illustration of the BFO thin film with upward ferroelectric polarization configuration around the conducting nanofilament wall formed by a biased CAFM tip; (b) PFM surface potential profile in the vicinity of the CAFM-formed conducting nanofilament wall; (c) PFM and (d) KFM images of the BFO thin film in the vicinity of the CAFM-formed conducting nanofilament wall; (e) schematic illustration showing the confinement of domain-wall motion inside the conducting nanofilament wall; (f) PFM image of the ferroelectric polarization nanobit confined by the conducting nanofilament wall.

than the conducting nanofilament region. Contrastively, a KFM image does not distinctively exhibit the conducting nanofilament wall between the upwardly polarized regions due to relatively poor resolution, compared with the PFM (Figure 4d).[18,19] We then placed the AFM tip near the conducting nanofilament wall to form the upwardly polarized nanobit. Once the ferroelectric polarization nanobit is reversed by the AFM tip, the domain wall of the nanobit spreads out. This is called "domain-wall motion" in the ferroelectric switching. As schematically depicted in Figure 4e, the AFM tip with a bias voltage of 0.5 V can induce a local region of the downward polarization, which is surrounded by the upwardly polarized domain (right-hand-side) and the conducting nanofilament wall (left-hand-side). The downwardly polarized domain can propagate through the surroundings having the opposite polarization. Interestingly, however, this downward polarization nanobit cannot spread out inside the conducting nanofilament wall with the surface potential of "0". Figure 4f shows a PFM image of the ferroelectric polarization nanobit confined by the conducting nanofilament wall. The distorted dark circle represents a region of the downward polarization induced by the CAFM bias. The left-hand-side of the asymmetric dark circle demonstrates the confinement of domain-wall motion by the conducting nanofilament wall.

We mainly attribute the confined ferroelectric domain motion to voltage-driven oxygen vacancies formed at the conducting filament region, although the detailed composition inside the conducting nanofilament still needs to be further clarified by more elaborate analysis techniques. As specified earlier, the oxygen vacancies have been considered to play a key role in forming the conducting filament path related to the unipolar resistive switching.[11−14] These oxygen vacancies have also been generally believed to be the main element resulting in the pinning of the ferroelectric domain wall related to polarization fatigue.[20−23] In other words, it implies that the ferroelectric domain-wall motion can be effectively restricted to the conducting filament wall. In addition, the highly conductive filaments lead to the electric field screening, where the domain-wall motion is indicative of being constrained. In the previous publications, accordingly, the conducting filaments in RRAMs have exhibited metallic characteristics.[17,24] This suggests that the ferroelectric domain cannot propagate into this wall region since the metallic-filament wall cannot possess any non-zero electric polarization as well. Therefore, it is worthy to note that the controllable conducting nanofilament wall formed by the CAFM techniques can be envisaged to manipulate the artificial shape of the ferroelectric domain, and thereby enables its individual nanometer-scale confinement.

CONCLUSIONS

In summary, we demonstrated the artificially controllable formation of conducting nanofilament walls via using the CAFM techniques inside the epitaxial $BiFeO_3$ thin films which exhibit the well-defined ferroelectric response and unipolar resistive switching behavior. More interestingly, we observed that the domain-wall motion is effectively confined within the conducting nanofilament wall during the polarization switching. These interesting features are envisaged to extend opportunities for nanoscale confinement of the domain-wall motion in the course of the ferroelectric switching.

ASSOCIATED CONTENT

Supporting Information

(1) X-ray diffraction data of the epitaxially grown $BiFeO_3$ thin film on the Nb-$SrTiO_3$(001) substrate; (2) reproducibility of the switching behavior of the Pt/$BiFeO_3$/Nb-$SrTiO_3$ capacitor. This material is available free of charge via the Internet at http://pubs.acs.org.

AUTHOR INFORMATION

Corresponding Authors

*E-mail: hanpos7@gmail.com.
*E-mail: jyson@khu.ac.kr.

Notes

The authors declare no competing financial interest.

ACKNOWLEDGMENTS

This work was supported by the National Research Foundation of Korea (NRF) grant funded by the Korea government (No. 2012R1A2A2A01046451).

REFERENCES

(1) Hill, N. A. Why Are There so Few Magnetic Ferroelectrics? *J. Phys. Chem. B* **2000**, *104*, 6694−6709.

(2) Lee, J.-H.; Choi, H. J.; Lee, D.; Kim, M. G.; Bark, C. W.; Ryu, S.; Oak, M.-A.; Jang, H. M. Variations of Ferroelectric Off-Centering Distortion and 3d-4p Orbital Mixing in La-doped $BiFeO_3$ Multiferroics. *Phys. Rev. B* **2010**, *82*, 045113.
(3) Wu, J.; Wang, J.; Xiao, D.; Zhu. Ferroelectric Behavior in Bismuth Ferrite Thin Films of Different Thickness. *ACS Appl. Mater. Interfaces* **2011**, *3*, 3261−3263.
(4) Jiang, K.; Zhu, J. J.; Wu, J. D.; Sun, J.; Hu, Z. G.; Chu, Z. H. Influences of Oxygen Pressure on Optical Properties and Interband Electronic Transitions in Multiferroic Bismuth Ferrite Nanocrystalline Films Grown by Pulsed Laser Deposition. *ACS Appl. Mater. Interfaces* **2011**, *3*, 4844−4852.
(5) Ryu, S.; Son, J. Y.; Shin, Y.-H.; Jang, H. M.; Scott, J. F. Polarization Switching Characteristics of Thin Films Epitaxially Grown on Pt/MgO at A Low Temperature. *Appl. Phys. Lett.* **2009**, *95*, 242902.
(6) Wu, J.; Wang, J.; Xiao, D.; Zhu, J. A. Method to Improve Electrical Properties of $BiFeO_3$ Thin Films. *ACS Appl. Mater. Interfaces* **2012**, *4*, 1182−1185.
(7) Kim, W.-H.; Son, J. Y. $BiFeO_3$ Nanodots Prepared via Dip-pen Lithography on Nb-Doped $SrTiO_3$ and Highly Ordered Pyrolytic Graphite Substrates. *Appl. Phys. Lett.* **2013**, *103*, 052905.
(8) Das, S. R.; Bhattacharya, P.; Choudhary, R. N. P.; Katiyar, R. S. Effect of La Substitution on Structural and Electrical Properties of $BiFeO_3$ Thin Film. *J. Appl. Phys.* **2006**, *99*, 066107.
(9) Wu, J.; Wang, J.; Xiao, D.; Zhu, Z. A Method to Improve Electrical Properties of $BiFeO_3$ Thin Films. *ACS Appl. Mater. Interfaces* **2011**, *3*, 1182−1185.
(10) Kim, W.-H.; Son, J. Y. The Effects of La Substitution on Ferroelectric Domain Structure and Multiferroic Properties of Epitaxially Grown $BiFeO_3$ Thin Films. *Appl. Phys. Lett.* **2013**, *103*, 132907.
(11) Wang, C.; Jin, K.-J.; Xu, Z.-T.; Wang, L.; Ge, C.; Lu, H.-B.; Guo, H.-Z.; He, M.; Yang, G.-Z. Switchable Diode Effect and Ferroelectric Resistive Switching in Epitaxial $BiFeO_3$ Thin Films. *Appl. Phys. Lett.* **2011**, *98*, 192901.
(12) Chen, S.-W.; Wu, J.-M. Unipolar Resistive Switching Behavior of $BiFeO_3$ Thin Films Prepared by Chemical Solution Deposition. *Thin Solid Films* **2010**, *519*, 499−504.
(13) Yin, K.; Li, M.; He, C.; Zhuge, F.; Chen, B.; Lu, W.; Pan, X.; Li, R.-W. Resistance Switching in Polycrystalline $BiFeO_3$ Thin Films. *Appl. Phys. Lett.* **2010**, *97*, 042101.
(14) Liu, L.; Zhang, S.; Luo, Y.; Yuan, G.; Liu, J.; Yin, J.; Liu, Z. Coexistence of Unipolar and Bipolar Resistive Switching in $BiFeO_3$ and $Bi_{0.8}Ca_{0.2}FeO_3$ Films. *J. Appl. Phys.* **2012**, *111*, 104103.
(15) Son, J. Y.; Shin, Y.-H.; Kim, H.; Cho, J. H.; Jang, H. Kelvin Probe Force Microscopy for Conducting Nanobits of NiO Thin Films. *Nanotechnology* **2010**, *21*, 215704.
(16) Son, J. Y.; Kim, D.-Y.; Kim, H.; Maeng, W. J.; Shin, Y.-S.; Shin, Y.-H. A HfO_2 Thin Film Resistive Switch Based on Conducting Atomic Force Microscopy. *Electrochem. Solid-State Lett.* **2011**, *14*, H311−H313.
(17) Son, J.Y.; Shin, Y.H. Direct Observation of Conducting Filaments on Resistive Switching of NiO Thin Films. *Appl. Phys. Lett.* **2008**, *92*, 222106.
(18) Jacobs, H. O.; Leuchtmann, P.; Homan, O. J.; Stemmer, A. Resolution and Contrast in Kelvin Probe Force Microscopy. *J. Appl. Phys.* **1998**, *84*, 1168−1173.
(19) Gil, A.; Colchero, J.; Gomez-Herrero, J.; Baro, A.M. Electrostatic Force Gradient Signal: Resolution Enhancement in Electrostatic Force Microscopy and Improved Kelvin Probe Microscopy. *Nanotechnology* **2003**, *14*, 332−340.
(20) He, L.; Vanderbilt, D. First-Principles Study of Oxygen-Vacancy Pinning of Domain Walls in $PbTiO_3$. *Phys. Rev. B* **2003**, *68*, 134103.
(21) Scott, J.; Dawber, M. Oxygen-Vacancy Ordering as a Fatigue Mechanism in Perovskite Ferroelectrics. *Appl. Phys. Lett.* **2000**, *76*, 3801−3803.
(22) Kimmel, A. V.; Weaver, P. M.; Cain, M. G.; Sushko, P. V. Defect-Mediated Lattice Relaxation and Domain Stability in Ferroelectric Oxides. *Phys. Rev. Lett.* **2012**, *109*, 117601.
(23) Park, C.; Chadi, D. Microscopic Study of Oxygen-Vacancy Defects in Ferroelectric Perovskites. *Phys. Rev. B* **1998**, *57*, R13961.
(24) Park, G.-S.; Li, X.-S.; Kim, D.-C.; Jung, R.-J.; Lee, M. J.; Seo, S. Observation of Electric-Field Induced Ni Filament Channels in Polycrystalline NiO_x Film. *Appl. Phys. Lett.* **2007**, *91*, 222103.